LUND UNIVERSITY

Frequency Selective Structures with Stochastic Deviations

Karlsson, Anders; Sjöberg, Daniel; Widenberg, Björn

2003

Total number of authors:
3

Frequency Selective Structures with Stochastic Deviations

Anders Karlsson, Daniel Sjöberg, and Björn Widenberg

Department of Electroscience
Electromagnetic Theory
Lund Institute of Technology
Sweden
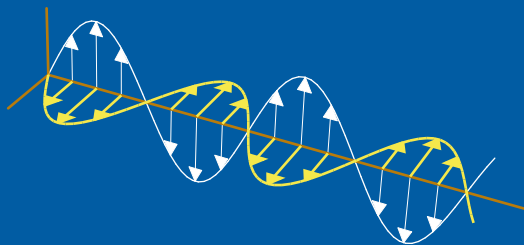
Anders Karlsson
Daniel Sjöberg
Björn Widenberg

Department of Electroscience
Electromagnetic Theory
Lund Institute of Technology
P.O. Box 118
SE-221 00 Lund
Sweden

Abstract

This paper deals with the performance of frequency selective structures with defects. A frequency selective structure is in this case a periodic pattern of apertures in a conducting plate. The plate can be of arbitrary thickness. The defects can be by deviations in the placing of the apertures, in the material parameters, or in the shape of the apertures. First the perturbation to the far-field pattern from a deviation in one aperture is analyzed. Then a statistical analysis is performed for a frequency selective structure where the apertures have a stochastic variation.

1 Introduction

A plane Frequency Selective Structure (FSS) is a periodic structure of infinitely many identical cells. The structure acts as a filter for an incident electromagnetic plane wave. For certain frequencies the induced currents in the cells interfere constructively such that all of the incident power is transmitted through the structure, whereas waves with other frequencies are partly, or entirely, reflected. This paper presents a simple method that can handle perturbations in the periodic pattern and that can estimate the effects these perturbations have on the filtering property. The method gives the surface fields, as well as the far-fields, from the perturbed region. It is also shown how a stochastic distribution of perturbations can be analyzed.

A number of different techniques have been developed during the years to analyze unperturbed frequency selective structures. The Method of Moments (MoM), *cf.* [5, 6], the Finite Difference Time-Domain (FDTD) technique [3], and the Finite Element Method (FEM) [2, 7], are three of the most common methods. The philosophy behind the perturbation method in this paper is that the numerical method and code used for the unperturbed periodic structure can, without modifications, be used to estimate the effects of perturbations to the periodic structure. Thus it is the chosen method for the unperturbed problem that sets the limits for what structures that can be handled. The methods mentioned above are very general and can *e.g.*, handle periodic patterns of metal strips, periodic patterns of apertures in conducing planes, and periodic patterns that include dielectric parts.

2 Unperturbed FSS

A frequency selective structure is a periodic pattern of identical cells. For simplicity it is assumed that the structure is parallel to the $xy-$plane and is periodic in the $x-$direction with a period a and in the perpendicular direction, the $y-$direction, with a period b. Structures that are periodic in non-perpendicular directions can be handled in the same manner, *cf.* [7]. The FSS has a finite thickness and is assumed to occupy the region $-h < z < 0$, *cf.* Figure 1. The FSS is assumed to be excited by an incident plane wave

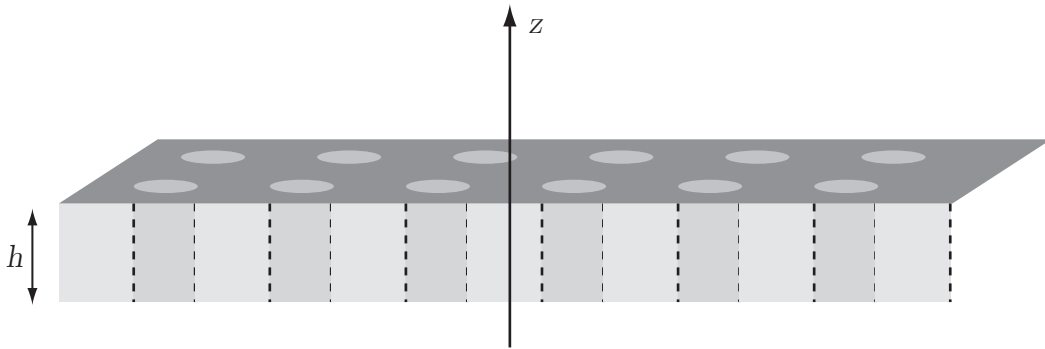$$\boldsymbol{E}^i(\boldsymbol{r}) = \boldsymbol{E}_0 \mathrm{e}^{\mathrm{i}\boldsymbol{k}_i \cdot \boldsymbol{r}}, \tag{2.1}$$

Figure 1: The frequency selective plate. The apertures may be filled with a dielectric material.

where the time dependence $\mathrm{e}^{-\mathrm{i}\omega t}$ is assumed and where $\boldsymbol{k}_i = (k_{ix}, k_{iy}, k_{iz})$ is the wave vector. For simplicity the incident wave is assumed to be incident from below, *i.e.*, with $k_{iz} > 0$. Due to the periodicity of the geometry, the reflected and transmitted fields are periodic vector functions in the $x-$ and $y-$directions. The periodicity is utilized by the numerical programs and the scattering region is reduced to one cell.

3 FSS with a single perturbed cell

If one or more cells are perturbed, a field that is not periodic will be superimposed the periodic field. This causes numerical problems since the scattering region no longer can be reduced to one cell. However, if the perturbation is small the interaction of the perturbed field with the surrounding cells can be neglected and the scattering region can be reduced to one cell. It is this approximation that makes the problem numerically feasible.

First consider an FSS where the cell S_k is perturbed, but all of the other cells are unperturbed. The total electric and magnetic fields at the surfaces of the cell are denoted $\boldsymbol{E}$, $\boldsymbol{H}$, the corresponding fields for the unperturbed case are denoted $\boldsymbol{E}^0$, $\boldsymbol{H}^0$, and the perturbation fields are denoted $\boldsymbol{E}^P$, $\boldsymbol{H}^P$. Thus

$$
\begin{aligned}
\boldsymbol{E} &= \boldsymbol{E}^0 + \boldsymbol{E}^P, \\
\boldsymbol{H} &= \boldsymbol{H}^0 + \boldsymbol{H}^P,
\end{aligned}
\tag{3.1}
$$

where the unperturbed fields are assumed to be known. The perturbation is assumed to be small enough for the following approximation to hold:

The tangential electric and magnetic surface fields on the surface of the perturbed cell are the same as the corresponding fields for an FSS where all of the cells are identical with the perturbed cell.

The approximation is referred to as the single cell approximation and is illustrated in Figure 2. The numerical examples in the numerical section indicate that this is a relevant approximation, even for quite large perturbations. There are two important features of this approximation; firstly the approximation is independent
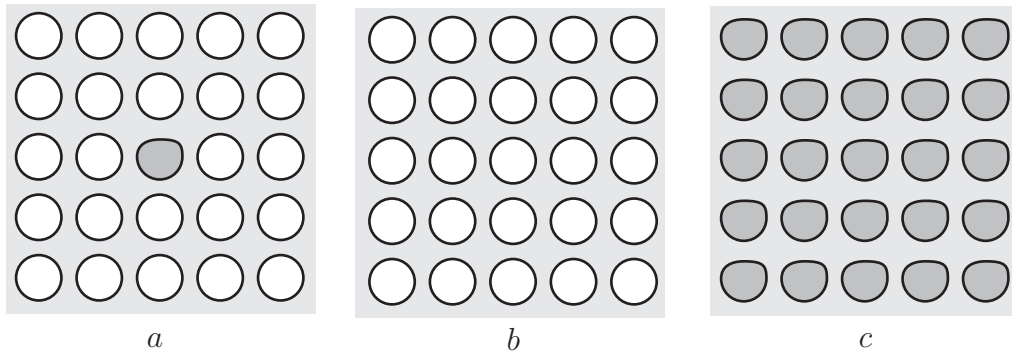
Figure 2: The single cell approximation. *a*) The periodic structure with one perturbed cell. *b*) The unperturbed periodic structure. *c*) The periodic structure with all of the cells perturbed. The surface field in the perturbed cell in *a* is approximately the same as the surface field in the corresponding cell in *c*. The perturbation of the surface field in the perturbed cell is approximately the difference between the surface fields in the corresponding cells in *c* and *b*.

of the numerical method that is used for the solution of the scattering problem, and secondly, the perturbation is obtained by numerically solving the surface fields for two different periodic structures. A numerical method that can handle the unperturbed structure can also handle the perturbation and hence no new numerical code is needed.

In the case of a large perturbation, the single cell approximation becomes inaccurate. It is then possible to introduce supercells in order to obtain the perturbed fields. A supercell is depicted in Figure 3. It consists of the perturbed cell and at least one of the cells surrounding the perturbed cell. To obtain the perturbation to the field one creates a periodic structure of supercells. The perturbed surface field of the perturbed cell is given by $\boldsymbol{E}^P = \boldsymbol{E} - \boldsymbol{E}^0$, where in this case $\boldsymbol{E}$ is the surface field from the periodic structure with each cell being a supercell. The supercells can be handled by an FDTD program for periodic structures without modification. Methods based on FEM or on MoM have to be slightly modified. In Appendix B it is seen how a method based on FEM is modified to handle supercells. Obviously the numerical calculations with supercells are more CPU-time consuming than without supercells. By comparing the single cell calculation with a supercell calculation, it should be possible to get a good estimate of the error. In the rest of the paper the approximation based on supercells is referred to as the supercell approximation, in contrast to the single cell approximation.

4 FSS with several perturbed cells

Now consider an FSS with more than one perturbed cell. If the perturbed cells are densely distributed, then if the supercell approximation is used, all of the cells in the supercell should be unaltered and a periodic structure with that supercell is
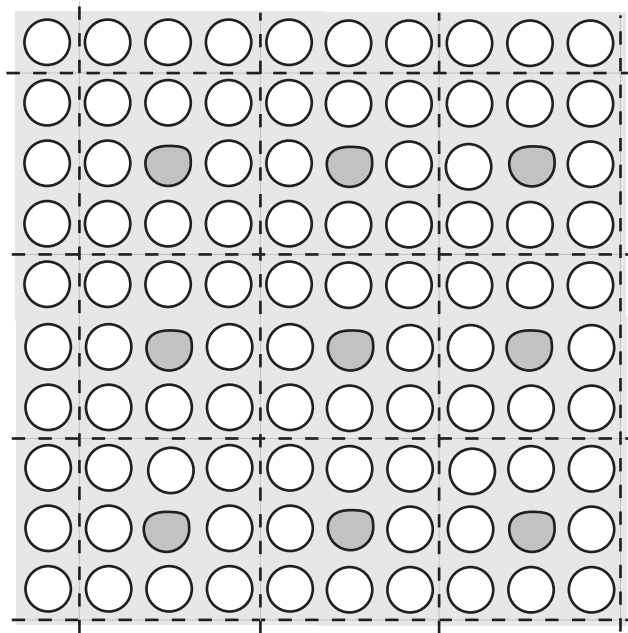
Figure 3: The supercell approximation. The surface field in the perturbed cell in the structure in Figure 2 is approximately the same as the surface field in the corresponding cell in the above structure. The approximation obtained from the supercell structure is better than the one obtained from the single cell approximation, *cf.* Figure 2.

formed, *cf.* Figure 4. Otherwise, if the perturbed cells are sparsely distributed and it is unlikely that two neighboring cells are perturbed, supercells where the other cells are unperturbed are accurate. When the perturbed cells have stochastic variations and when their distribution is stochastic the methods described in Section 3 are applicable.

5 Far-field amplitude

The perturbation of the far-field can be determined from the integral representation of the field. First consider an FSS with no dielectric layers. The perturbation to the far-field from one perturbed cell yields

$$\boldsymbol{E}_s(\boldsymbol{r}) = \frac{\mathrm{e}^{\mathrm{i}kr}}{kr}\boldsymbol{F}(\hat{\boldsymbol{r}}). \tag{5.1}$$

The far-field amplitude is different above and below the FSS. In both cases the expression for the perturbation reads

$$\boldsymbol{F}^P(\hat{\boldsymbol{r}}) = \mathrm{i}\frac{k^2}{4\pi}\hat{\boldsymbol{r}} \times \iint_{S_k} [\hat{\boldsymbol{n}} \times \boldsymbol{E}^P(\boldsymbol{r}') - \eta_0\hat{\boldsymbol{r}} \times (\hat{\boldsymbol{n}} \times \boldsymbol{H}^P(\boldsymbol{r}'))]\mathrm{e}^{-\mathrm{i}k\hat{\boldsymbol{r}}\cdot\boldsymbol{r}'}\,\mathrm{d}S'. \tag{5.2}$$

For the far-field above the FSS ($z > 0$) S_k is the surface of the cell at $z = 0$ and $\hat{\boldsymbol{n}} = \hat{\boldsymbol{z}}$, and for the far-field below the FSS ($z < -h$) S_k is the surface of the cell at $z = -h$ and $\hat{\boldsymbol{n}} = -\hat{\boldsymbol{z}}$.

6   Translated aperture

The simplest case of perturbation is a displacement of the cell number p a vector $\delta \boldsymbol{r}_p = (\delta x_p, \delta y_p, 0)$. The displacement is assumed to be small enough for the single cell approximation to hold. The difference between the case with all of the apertures displaced and the case with no cells displaced is simply due to the translation of the coordinate system. The surface fields of the displaced cell are given by

$$
\begin{aligned}
\boldsymbol{E}_T(\boldsymbol{r}) &= \mathrm{e}^{\mathrm{i}\boldsymbol{k}_i \cdot \delta \boldsymbol{r}_p} \boldsymbol{E}_T^0(\boldsymbol{r}), \\
\boldsymbol{H}_T(\boldsymbol{r}) &= \mathrm{e}^{\mathrm{i}\boldsymbol{k}_i \cdot \delta \boldsymbol{r}_p} \boldsymbol{H}_T^0(\boldsymbol{r}),
\end{aligned} \tag{6.1}
$$

where again $\boldsymbol{E}^0$ and $\boldsymbol{H}^0$ are the tangential field for the unperturbed cell. The corresponding perturbations to the surface fields are

$$
\begin{aligned}
\boldsymbol{E}_T^P(\boldsymbol{r}) &= (\mathrm{e}^{\mathrm{i}\boldsymbol{k}_i \cdot \delta \boldsymbol{r}_p} - 1)\boldsymbol{E}_T^0(\boldsymbol{r}), \\
\boldsymbol{H}_T^P(\boldsymbol{r}) &= (\mathrm{e}^{\mathrm{i}\boldsymbol{k}_i \cdot \delta \boldsymbol{r}_p} - 1)\boldsymbol{E}_T^0(\boldsymbol{r}).
\end{aligned} \tag{6.2}
$$

The far-field amplitude is given by

$$
\boldsymbol{F}(\hat{\boldsymbol{r}}) = \mathrm{e}^{\mathrm{i}\boldsymbol{q} \cdot \delta \boldsymbol{r}_p} \boldsymbol{F}^0(\hat{\boldsymbol{r}}), \tag{6.3}
$$

where $\boldsymbol{F}^0$ is the far-field amplitude for a cell that is not translated and where

$$
\boldsymbol{q} = \boldsymbol{k}_i - k\hat{\boldsymbol{r}}. \tag{6.4}
$$

Hence k is the wave number and $\hat{\boldsymbol{r}} = \boldsymbol{r}/r$. In all directions where $\boldsymbol{q} \cdot \delta \boldsymbol{r}_p = n2\pi$ the perturbation to the far-field is zero. Since $\delta \boldsymbol{r}_p$ is small this only happens for $n = 0$, i.e., in the forward direction ($\boldsymbol{k}_i - k\hat{\boldsymbol{r}} = \boldsymbol{0}$) and in the specular reflection direction, $k\hat{\boldsymbol{r}} = (k_{ix}, k_{iy}, -k_{iz})$. If the first order term in powers of delta is kept, it is seen that

$$
\begin{aligned}
\boldsymbol{E}_T^P(\boldsymbol{r}) &= \mathrm{i}(\boldsymbol{k}_i \cdot \delta \boldsymbol{r}_p)\boldsymbol{E}_T^0(\boldsymbol{r}), \\
\boldsymbol{H}_T^P(\boldsymbol{r}) &= \mathrm{i}(\boldsymbol{k}_i \cdot \delta \boldsymbol{r}_p)\boldsymbol{E}_T^0(\boldsymbol{r}), \\
\boldsymbol{F}^P(\hat{\boldsymbol{r}}) &= \mathrm{i}(\boldsymbol{k}_i \cdot \delta \boldsymbol{r}_p)\boldsymbol{F}^0(\hat{\boldsymbol{r}}).
\end{aligned} \tag{6.5}
$$

The perturbations to the far-field in the forward direction and in the specular reflection direction are of second order in $\delta \boldsymbol{r}_p$ and can not be obtained by the single cell approximation. They require a supercell approximation.

7   FSS with a dielectric layer

Often the metallic FSS is coated with a dielectric layer. For simplicity it is assumed that the upper part of the metallic surface is at $z = 0$ and that the layer $0 < z < z_0$

is occupied by a homogeneous dielectric material with permittivity ε_r. There are two ways to obtain the perturbation to the far-field when the layer is present. The first alternative is to calculate the surface fields on the upper surface of the dielectric layer, *i.e.*, at $z = z_0$, directly. This is probably a good approximation if the layer is much thinner than the width of the cell. If the layer is thick it is better to calculate the surface fields on the metal surface and then calculate the far-field amplitude. To take the effect of the dielectric layer into account one may use an expansion in plane waves, in combination with the method of stationary phase. The expression for the far-field in the upper half space, $z > z_0$ is given by

$$
\begin{aligned}
\boldsymbol{E}_0(\boldsymbol{r}) &= \frac{\boldsymbol{F}(\hat{\boldsymbol{r}})}{kr} \mathrm{e}^{\mathrm{i}kr}, \\
\boldsymbol{F}(\hat{\boldsymbol{r}}) &= 2\pi \mathrm{i} \sum_{j=1}^{2} a_j(\boldsymbol{k}_1) T_j(\boldsymbol{k}) \boldsymbol{\phi}_j(\boldsymbol{k}; \boldsymbol{0}),
\end{aligned}
\tag{7.1}
$$

where T_j are the transmission coefficients for the dielectric layer, $\boldsymbol{\phi}_j$ are vector plane waves, and a_j are plane wave coefficients. The explicit expressions for these quantities and a derivation of the expressions are given in Appendix A.

8 Stochastic variation of several apertures

Consider an FSS with a number of perturbed cells. If the apertures are not identical, the transmitted and reflected power are affected. Consider the case when the shape and position of the cells have some stochastic variation. The variation is considered to be small enough for the approximations done in the previous section to hold. The far-field amplitude above the structure from cell number n is given by

$$
\boldsymbol{F}_n(\hat{\boldsymbol{r}}) = \boldsymbol{F}^0(\hat{\boldsymbol{r}}) + \boldsymbol{F}_n^P(\hat{\boldsymbol{r}}) = \boldsymbol{F}^0(\hat{\boldsymbol{r}}) + \delta\boldsymbol{F}^0(\hat{\boldsymbol{r}}) + \Delta\boldsymbol{F}_n(\hat{\boldsymbol{r}}),
\tag{8.1}
$$

where $\boldsymbol{F}^0(\hat{\boldsymbol{r}})$ is the far-field amplitude for one cell of the unperturbed structure, $\delta\boldsymbol{F}^0(\hat{\boldsymbol{r}})$ is the mean value of the perturbation of the far-field, and $\Delta\boldsymbol{F}_n(\hat{\boldsymbol{r}})$ is the part of the perturbed far-field that has mean value zero. Thus

$$
< \boldsymbol{F}_n(\hat{\boldsymbol{r}}) > = \boldsymbol{F}^0(\hat{\boldsymbol{r}}) + \delta\boldsymbol{F}^0(\hat{\boldsymbol{r}}).
\tag{8.2}
$$

Let $\boldsymbol{r}_n$ be the location of the centers of the cells in the FSS and let $\boldsymbol{k}_s = k\hat{\boldsymbol{r}}$ be the wave vector of the scattered field. The centers of the cells are defined by the unperturbed structure and are not affected by a perturbation of the cell. Let the structure be finite with $N = N_x \times N_y$ cells and disregard from the fact that the cells at the border of the structure are different. Following [4] the average electromagnetic power flow density from the FSS is given by

$$
\frac{1}{2\eta_0} < |\boldsymbol{E}(\boldsymbol{r})|^2 > = \frac{1}{2\eta_0 k^2 r^2} < |\sum_{n=1}^{N} \mathrm{e}^{\mathrm{i}\boldsymbol{q}\cdot\boldsymbol{r}_n} \boldsymbol{F}_n(\hat{\boldsymbol{r}})|^2 >,
\tag{8.3}
$$

where $\boldsymbol{q} = \boldsymbol{k}_i - k\hat{\boldsymbol{r}}$. The following relation holds

$$< |\sum_{n=1}^{N} \mathrm{e}^{\mathrm{i}\boldsymbol{q}\cdot\boldsymbol{r}_n} \boldsymbol{F}_n(\hat{\boldsymbol{r}})|^2 >= N < |\Delta\boldsymbol{F}_n(\hat{\boldsymbol{r}})|^2 > + |\boldsymbol{F}^0(\hat{\boldsymbol{r}}) + \delta\boldsymbol{F}^0(\hat{\boldsymbol{r}})|^2 \sum_{n=1}^{N}\sum_{n'=1}^{N} \mathrm{e}^{\mathrm{i}\boldsymbol{q}\cdot(\boldsymbol{r}_n - \boldsymbol{r}_{n'})}.$$

(8.4)

The sum on the right hand side can be summed. Since n is a multiindex and $\boldsymbol{r}_n = (n_x a, n_y b, 0)$ it is seen that

$$|\sum_{n=1}^{N} \mathrm{e}^{\mathrm{i}\boldsymbol{q}\cdot\boldsymbol{r}_n}|^2 = \sum_{n=1}^{N}\sum_{n'=1}^{N} \mathrm{e}^{\mathrm{i}\boldsymbol{q}\cdot(\boldsymbol{r}_n - \boldsymbol{r}_{n'})} = |\sum_{n_x=1}^{N_x} \mathrm{e}^{\mathrm{i}q_x n_x a}|^2 |\sum_{n_y=1}^{N_y} \mathrm{e}^{\mathrm{i}q_y n_y b}|^2. \qquad (8.5)$$

Each series is summed as

$$|\sum_{n_x=-N_x}^{N_x} \mathrm{e}^{\mathrm{i}q_x n_x a}|^2 = |\frac{\sin(N_x q_x a/2)}{\sin(q_x a/2)}|^2, \qquad (8.6)$$

and it follows that

$$|\sum_{n=1}^{N} \mathrm{e}^{\mathrm{i}\boldsymbol{q}\cdot\boldsymbol{r}_n}|^2 = |\frac{\sin(N_x q_x a/2)}{\sin(q_x a/2)}|^2 |\frac{\sin(N_y q_y b/2)}{\sin(q_y b/2)}|^2. \qquad (8.7)$$

As the structure becomes infinitely large in both the $x-$ and $y-$direction then using Feijer's method, *cf.* [1]

$$\lim_{N_x\to\infty} \frac{1}{N_x}\left(\frac{\sin(N_x q_x a/2)}{\sin(q_x a/2)}\right)^2 = 2\pi\delta(q_x), \qquad (8.8)$$

it is seen that

$$\lim_{N\to\infty} \frac{1}{N}|\sum_{n=1}^{N} \mathrm{e}^{\mathrm{i}\boldsymbol{q}\cdot\boldsymbol{r}_n}|^2 = 4\pi^2\delta(q_x)\delta(q_y). \qquad (8.9)$$

The scattered power per unit solid angle is

$$U_s(\hat{\boldsymbol{r}}) = \frac{1}{2\eta_0} < r^2|\boldsymbol{E}_s(\boldsymbol{r})|^2 > . \qquad (8.10)$$

The incident power is given by

$$P_i = \frac{1}{2\eta_0}|\boldsymbol{E}_0|^2 NA|\hat{\boldsymbol{k}}_i \cdot \hat{\boldsymbol{z}}|. \qquad (8.11)$$

The corresponding power scattering coefficient per unit solid angle (differential scattering cross section) reads

$$\frac{U_s(\hat{\boldsymbol{r}})}{P_i} = \frac{1}{k^2 A|\hat{\boldsymbol{k}}_i \cdot \hat{\boldsymbol{z}}|}\left(\frac{< |\Delta\boldsymbol{F}_n(\hat{\boldsymbol{r}})| >^2}{|\boldsymbol{E}_0|^2}\right.$$
$$\left. + \frac{|\boldsymbol{F}^0(\hat{\boldsymbol{r}}) + \delta\boldsymbol{F}^0(\hat{\boldsymbol{r}})|^2}{|\boldsymbol{E}_0|^2}\frac{1}{N}\left(\frac{\sin(N_x q_x a/2)}{\sin(q_x a/2)}\right)^2\left(\frac{\sin(N_y q_y b/2)}{\sin(q_y b/2)}\right)^2\right). \qquad (8.12)$$

As the structure becomes infinitely large this becomes

$$\frac{U_s(\hat{\boldsymbol{r}})}{P_i} = \frac{1}{k^2 A|\hat{\boldsymbol{k}}_i \cdot \hat{\boldsymbol{z}}|} \left(\frac{<|\Delta\boldsymbol{F}_n|>^2}{|\boldsymbol{E}_0|^2} + \frac{|\boldsymbol{F}^0(\hat{\boldsymbol{r}}) + \delta\boldsymbol{F}^0(\hat{\boldsymbol{r}})|^2}{|\boldsymbol{E}_0|^2} 4\pi^2\delta(q_x)\delta(q_y) \right). \quad (8.13)$$

When the perturbation is a translation $\delta\boldsymbol{r}_n = (\delta x_n, \delta y_n, 0)$ explicit expressions can be obtained. Thus the far-field amplitude from one cell is

$$\boldsymbol{F}_n(\hat{\boldsymbol{r}}) = \mathrm{e}^{-\mathrm{i}\boldsymbol{q}\cdot\delta\boldsymbol{r}_n}\boldsymbol{F}^0(\hat{\boldsymbol{r}}), \quad (8.14)$$

and

$$\begin{aligned}
\boldsymbol{F}^0(\hat{\boldsymbol{r}}) + \delta\boldsymbol{F}^0(\hat{\boldsymbol{r}}) &= <\mathrm{e}^{-\mathrm{i}\boldsymbol{q}\cdot\delta\boldsymbol{r}_n}>\boldsymbol{F}^0(\hat{\boldsymbol{r}}), \\
\Delta\boldsymbol{F}_n(\hat{\boldsymbol{r}}) &= (\mathrm{e}^{-\mathrm{i}\boldsymbol{q}\cdot\boldsymbol{\delta r}_n} - <\mathrm{e}^{-\mathrm{i}\boldsymbol{q}\cdot\delta\boldsymbol{r}_n}>)\boldsymbol{F}^0(\hat{\boldsymbol{r}}).
\end{aligned} \quad (8.15)$$

Then

$$\begin{aligned}
\frac{U_s(\hat{\boldsymbol{r}})}{P_i} =& \frac{|\boldsymbol{F}^0(\hat{\boldsymbol{r}})|^2}{k^2 A|\boldsymbol{E}_0|^2|\hat{\boldsymbol{k}}_i \cdot \hat{\boldsymbol{z}}|} \left(1 - |<\mathrm{e}^{-\mathrm{i}\boldsymbol{q}\cdot\delta\boldsymbol{r}_n}>|^2 \right. \\
&\left. +|<\mathrm{e}^{-\mathrm{i}\boldsymbol{q}\cdot\delta\boldsymbol{r}_n}>|^2\frac{1}{N} \left(\frac{\sin(N_x q_x a/2)}{\sin(q_x a/2)} \right)^2 \left(\frac{\sin(N_y q_y b/2)}{\sin(q_y b/2)} \right)^2 \right).
\end{aligned} \quad (8.16)$$

As the structure becomes infinitely large this becomes

$$\frac{U_s(\hat{\boldsymbol{r}})}{P_i} = \frac{|\boldsymbol{F}^0(\hat{\boldsymbol{r}})|^2}{k^2 A|\boldsymbol{E}_0|^2|\hat{\boldsymbol{k}}_i \cdot \hat{\boldsymbol{z}}|} \left(1 - |<\mathrm{e}^{-\mathrm{i}\boldsymbol{q}\cdot\delta\boldsymbol{r}_n}>|^2 + |<\mathrm{e}^{-\mathrm{i}\boldsymbol{q}\cdot\delta\boldsymbol{r}_n}>|^2 4\pi^2\delta(q_x)\delta(q_y) \right). \quad (8.17)$$

9 Numerical examples

In this section it is indicated that the perturbed surface fields are localized fields that in most cases are negligible in the cells surrounding the perturbed cell. This is done by calculating the perturbation to the tangential electric and magnetic fields on the surface of the perturbed cell, using the single cell approximation. In this case the unperturbed cell consists of a circular aperture in a perfectly conducting plate. The thickness of the plate is one mm, the radius of the aperture is 15 mm, the cell is quadratic 23×23 mm, and the center of the aperture coincides with the center of the cell. The incident electric field is a linearly polarized plane wave at normal incidence, with the electric field in the $x-$direction, *i.e.*, the horizontal direction in the figure. The frequency is 10 GHz. The perturbed cell has its aperture displaced either a distance 4 mm to the right or 4 mm upwards.

The surface fields were calculated by a method that utilizes FEM in combination with a mode matching technique, *cf.* [7]. The perturbed fields, $\boldsymbol{E}_T^P(\boldsymbol{r})$ and $\boldsymbol{H}_T^P(\boldsymbol{r})$, were obtained by first solving the unperturbed periodic case to get $\boldsymbol{E}_T^0(\boldsymbol{r})$ and $\boldsymbol{H}_T^0(\boldsymbol{r})$, and then solving the periodic case with all cells displaced to obtain $\boldsymbol{E}_T(\boldsymbol{r})$ and $\boldsymbol{H}_T(\boldsymbol{r})$. It was checked that the latter fields only differ by a phase shift $\boldsymbol{k} \cdot \delta\boldsymbol{r}$ compared to the unperturbed fields, *cf.* Subsection 6. The resulting fields,
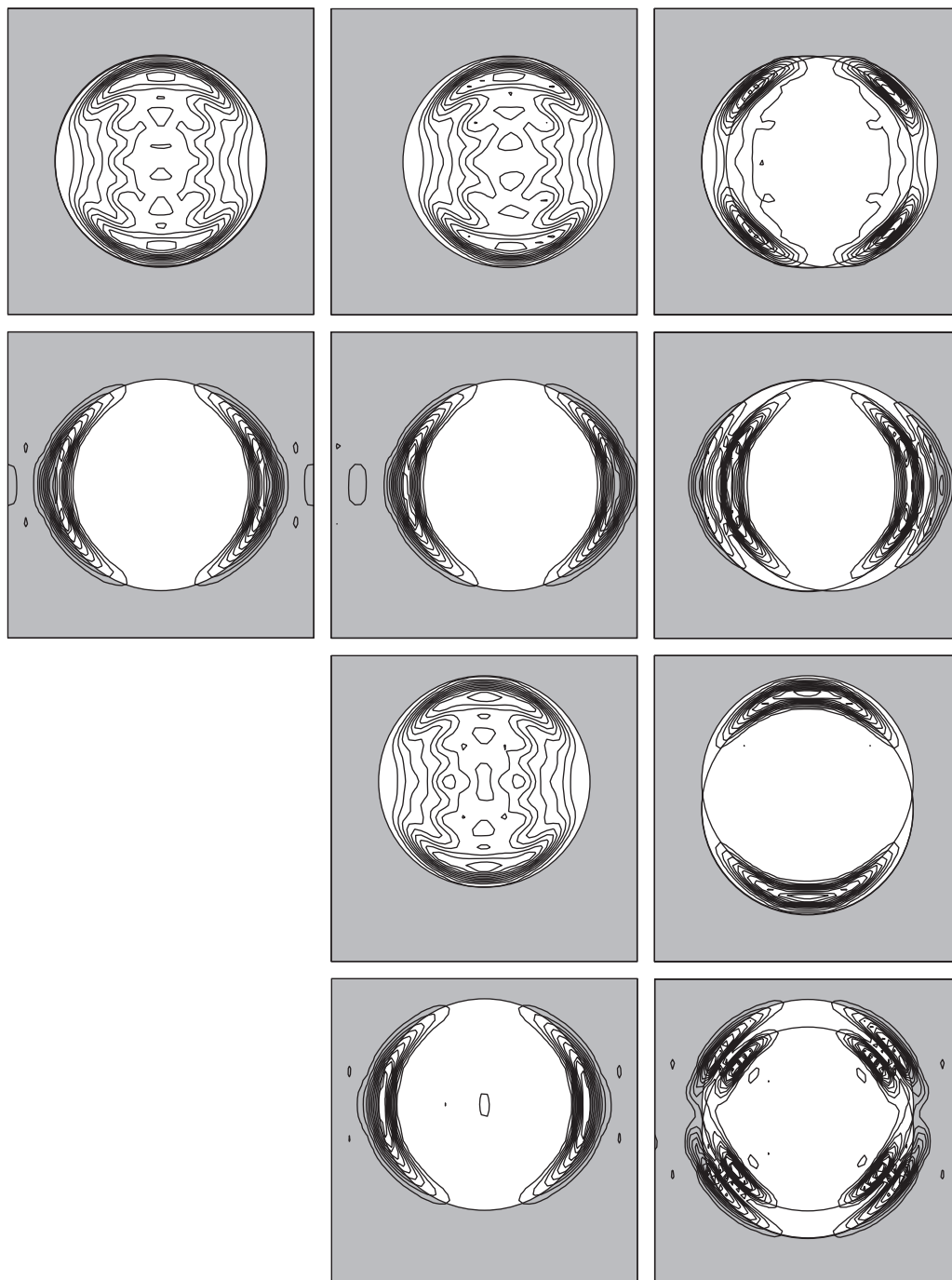
Figure 4: The surface fields of the tangential electric and magnetic fields of cells with circular apertures. The incident field, the geometry, and the figures are described in Section 9.

$\boldsymbol{E}_T^P(\boldsymbol{r})$ and $\boldsymbol{H}_T^P(\boldsymbol{r})$, are shown in Figure 4. Let (i,j) denote the subfigure in row i and colon j. The unperturbed tangential electric field $\boldsymbol{E}_T^0$ is shown in figure (1,1) and the corresponding magnetic field $\boldsymbol{H}_T^0$ in figure (2,1). In figures (1,2) and (2,2) the tangential electric and magnetic fields $\boldsymbol{E}_T$ and $\boldsymbol{H}_T$ are shown for the periodic case with all of the apertures displaced horizontally a vector $\delta\boldsymbol{r} = \delta x \hat{\boldsymbol{x}}$, with $\delta x = 4\,\text{mm}$. The perturbation to the tangential electric and magnetic fields, $\boldsymbol{E}_T^P$ and $\boldsymbol{H}_T^P$, are shown in figures (1,3) and (2,3), respectively. The case with a perturbation $\delta\boldsymbol{r} = \delta y \hat{\boldsymbol{y}}$ with $\delta y = 4\,\text{mm}$ is shown in figures (3,2), (3,3), (4,2), and (4,4). Then the figures (3,2) and (4,2) depict the electric and magnetic fields for the periodic case with all of the apertures displaced and figures (4,2) and (4,3) depict the perturbations to the tangential electric and magnetic fields.

As seen from the plots in Figure 4, the perturbation of the fields are concentrated to the area close to the edge of the aperture. The perturbation is close to zero at the border between the cells.

It is anticipated that the perturbation to the surface fields are negligible in the other cells. To check this, one should make a calculation with supercells. This can be done by the method described in Appendix B and such calculations are to be presented in a coming paper.

10 Acknowledgments

Appendix A FSS with dielectric layers

Consider the case where there is a dielectric layer of thickness z_0 above the FSS. The tangential components of $\boldsymbol{E}$ and $\boldsymbol{H}$ are considered to be known on the surface $z = 0$ of one cell. The corresponding far-field amplitude is to be determined. Let the surface of the cell be at $z = 0$. The interface between the dielectric layer and air is at $z = z_0$. The quantities defined in the region $0 < z < z_0$ are denoted with an index 1 and quantities in the region $z > z_0$ have no index. A plane wave expansion of the upwards travelling field in region 1 is given by

$$\boldsymbol{E}_1(\boldsymbol{r}) = \int_{-\infty}^{\infty}\int_{-\infty}^{\infty}\sum_{j=1}^{2}\boldsymbol{\phi}_j(\boldsymbol{k}_1;\boldsymbol{r})a_j(\boldsymbol{k}_1)dk_xdk_y, \tag{A.1}$$

where the plane waves are given by

$$\boldsymbol{\phi}_1(\boldsymbol{k}_1;\boldsymbol{r}) = -\hat{\boldsymbol{\beta}}\frac{\mathrm{i}}{4\pi}\mathrm{e}^{\mathrm{i}\boldsymbol{k}_1\cdot\boldsymbol{r}},$$
$$\boldsymbol{\phi}_2(\boldsymbol{k}_1;\boldsymbol{r}) = -\hat{\boldsymbol{\alpha}}\frac{1}{4\pi}\mathrm{e}^{\mathrm{i}\boldsymbol{k}_1\cdot\boldsymbol{r}}. \tag{A.2}$$

Here β and α are the spherical angles such that

$$\boldsymbol{k}_1 = k_1(\sin\alpha\cos\beta, \sin\alpha\sin\beta, \cos\alpha), \tag{A.3}$$

and

$$\begin{aligned} \hat{\boldsymbol{\beta}} &= (-\sin\beta, \cos\beta, 0), \\ \hat{\boldsymbol{\alpha}} &= (\cos\alpha\cos\beta, \cos\alpha\sin\beta, -\sin\alpha), \end{aligned} \tag{A.4}$$

where $\cos\alpha > 0$ since the wave is travelling upwards. The plane waves satisfy

$$\begin{aligned} \nabla \times \boldsymbol{\phi}_1 &= k_1\boldsymbol{\phi}_2, \\ \nabla \times \boldsymbol{\phi}_2 &= k_1\boldsymbol{\phi}_1. \end{aligned} \tag{A.5}$$

The plane wave expansion of the Green dyadic reads

$$\boldsymbol{G}(\boldsymbol{r}, \boldsymbol{r}'; k_1) = 2\mathrm{i} \sum_{j=1}^{2} \int_{-\infty}^{\infty} \int_{-\infty}^{\infty} \frac{1}{k_{1z}} \boldsymbol{\phi}_j(\boldsymbol{k}_1; \boldsymbol{r}) \boldsymbol{\phi}_j^\dagger(\boldsymbol{k}_1; \boldsymbol{r}') dk_x dk_y, \tag{A.6}$$

where the dagger means that i is exchanged for $-\mathrm{i}$ in Eq. (A.2). From the integral representation of the electric field and the expansion of the Green dyadic the plane wave expansion coefficients are obtained as

$$a_1(\boldsymbol{k}_1) = 2\mathrm{i}\frac{1}{k_{1z}} \left(\int_S k_1(\hat{\boldsymbol{n}} \times \boldsymbol{E}_1) \cdot \boldsymbol{\phi}_2^\dagger(\boldsymbol{k}_1; \boldsymbol{r}') + (\hat{\boldsymbol{n}} \times \nabla' \times \boldsymbol{E}_1) \cdot \boldsymbol{\phi}_1^\dagger(\boldsymbol{k}_1; \boldsymbol{r}') \, \mathrm{d}S' \right),$$

$$a_2(\boldsymbol{k}_1) = 2\mathrm{i}\frac{1}{k_{1z}} \left(\int_S k_1(\hat{\boldsymbol{n}} \times \boldsymbol{E}_1) \cdot \boldsymbol{\phi}_1^\dagger(\boldsymbol{k}_1; \boldsymbol{r}') + (\hat{\boldsymbol{n}} \times \nabla' \times \boldsymbol{E}_1) \cdot \boldsymbol{\phi}_2^\dagger(\boldsymbol{k}_1; \boldsymbol{r}') \, \mathrm{d}S' \right). \tag{A.7}$$

The transmitted field is obtained by utilizing the boundary conditions at the plane surface at $z = z_0$

$$\boldsymbol{E}_0(\boldsymbol{r}) = \frac{1}{k} \int_{-\infty}^{\infty} \frac{1}{k_{0z}} \int_{-\infty}^{\infty} \sum_{j=1}^{2} a_j(\boldsymbol{k}_1) T_j(\boldsymbol{k}) \boldsymbol{\phi}_j(\boldsymbol{k}; \boldsymbol{r}) dk_x dk_y, \tag{A.8}$$

where $\boldsymbol{k}_1$ and $\boldsymbol{k}$ are related by Snell's law, i.e.,

$$\begin{aligned} k_{0x} &= k_{1x} = k_x, \qquad k_{0y} = k_{1y} = k_y, \\ k_{0z} &= \sqrt{k^2 - k_x^2 - k_y^2}, \qquad k_{1z} = \sqrt{k_1^2 - k_x^2 - k_y^2}. \end{aligned} \tag{A.9}$$

The transmission coefficients are given by

$$\begin{aligned} T_1 &= \frac{2k_{1z}}{k_{1z} + k_{0z}} \exp(\mathrm{i}z_0(k_{1z} - k_{0z})), \\ T_2 &= \frac{2kk_1k_{1z}}{k^2k_{1z} + k_1^2k_{0z}} \exp(\mathrm{i}z_0(k_{1z} - k_{0z})). \end{aligned} \tag{A.10}$$

The far-field amplitude is obtained by letting $r = |\boldsymbol{r}| \to \infty$. The Fourier integral is then evaluated by the stationary phase method. The result is

$$\boldsymbol{E}_0(\boldsymbol{r}) = \frac{\boldsymbol{F}(\hat{\boldsymbol{r}})}{kr}\mathrm{e}^{\mathrm{i}kr},$$

$$\boldsymbol{F}(\hat{\boldsymbol{r}}) = 2\pi\mathrm{i}\sum_{j=1}^{2} a_j(\boldsymbol{k}_1)T_j(\boldsymbol{k})\boldsymbol{\phi}_j(\boldsymbol{k};\boldsymbol{0}). \tag{A.11}$$

A.1 Stationary phase method

The electric field reads

$$\boldsymbol{E}(\boldsymbol{r}) = \int\limits_{-\infty}^{\infty}\int\limits_{-\infty}^{\infty} \boldsymbol{f}(\boldsymbol{k})\mathrm{e}^{\mathrm{i}(k_x x + k_z z)}dk_x \mathrm{e}^{\mathrm{i}k_y y}dk_y. \tag{A.12}$$

When $r \to \infty$ the integral can be evaluated by the stationary phase method. The k_x integral is considered first. The exponent has a stationary point when

$$\frac{d}{dk_x}(k_x x + k_z z) = x - \frac{k_x}{k_z}z = 0, \tag{A.13}$$

i.e., when $k_x/k_z = x/z$. The second derivative of the exponent is

$$\frac{d^2}{dk_x^2}(k_x x + k_z z) = -\frac{z}{k_z} - \frac{k_x^2}{k_z^3}z = -\frac{z}{k_z}\left(1 + \frac{x^2}{z^2}\right). \tag{A.14}$$

The integral is then given by

$$\boldsymbol{E}_0(\boldsymbol{r}) = \int\limits_{-\infty}^{\infty}\left(\frac{2\pi\mathrm{i}}{-z/k_z(1 + x^2/z^2)}\right)^{1/2}\boldsymbol{f}(\boldsymbol{k})\mathrm{e}^{\mathrm{i}k_z(x^2/z+z)}\mathrm{e}^{\mathrm{i}k_y y}dk_y, \tag{A.15}$$

where

$$k_z = \sqrt{\frac{k^2 - k_y^2}{x^2 + z^2}}z. \tag{A.16}$$

The stationary point is obtained from

$$\frac{d}{dk_y}(k_y y + k_z(x^2/z + z))) = y - \frac{k_y}{\sqrt{k^2 - k_y^2}}\sqrt{x^2 + z^2} = 0. \tag{A.17}$$

Hence

$$\frac{k_x}{x} = \frac{k_y}{y} = \frac{k_z}{z} = \frac{k}{r}. \tag{A.18}$$

The second derivative of the exponent yields

$$\frac{d^2}{dk_y^2}(k_y y + k_z(x^2/z + z))) = -\frac{rk}{k^2 - k_z^2}. \tag{A.19}$$
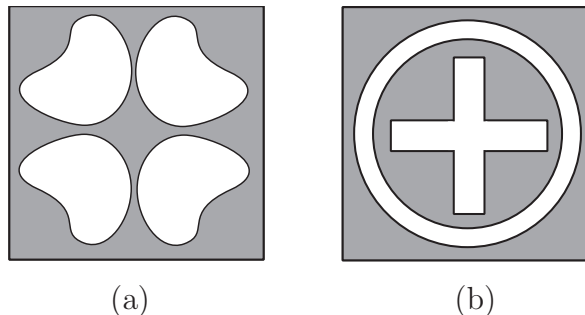
(a)　　　　　　　　　　　(b)

Figure 5: Two examples of unit cells that contain more than one aperture: (a) Four apertures. (b) Two apertures: an annular and a crossed dipole aperture.

The integral is then given by

$$\boldsymbol{E}_0(\boldsymbol{r}) = \left(\frac{2\pi\mathrm{i}}{-z/k_z(1+x^2/z^2)}\right)^{1/2}\left(-2\pi\mathrm{i}\frac{k^2-k_y^2}{rk}\right)^{1/2}\boldsymbol{f}(\boldsymbol{k})\mathrm{e}^{\mathrm{i}k_z(x^2/z+z)}\mathrm{e}^{\mathrm{i}k_y y}. \quad (\text{A.20})$$

Since $k_x/x = k_y/y = k_z/z$ it follows that $\boldsymbol{k}\cdot\boldsymbol{r} = kr$ and $k_x/x = k/r$. Hence

$$\boldsymbol{E}_0(\boldsymbol{r}) = \frac{2\pi\mathrm{i}k_z}{r}\boldsymbol{f}(\boldsymbol{k})\mathrm{e}^{\mathrm{i}kr}, \quad (\text{A.21})$$

where

$$\boldsymbol{f}(\boldsymbol{k}) = \frac{1}{kk_z}\sum_{j=1}^{2} a_j(\boldsymbol{k}_1)T_j(\boldsymbol{k})\boldsymbol{\phi}_j(\boldsymbol{k};\boldsymbol{0}). \quad (\text{A.22})$$

The final expression is

$$\boldsymbol{E}_0(\boldsymbol{r}) = \frac{2\pi\mathrm{i}k_z}{r}\boldsymbol{f}(\boldsymbol{k})\mathrm{e}^{\mathrm{i}kr}. \quad (\text{A.23})$$

Appendix B　Supercells

In [7] a method that can handle frequency selective structures with apertures was described. The method is based on FEM and expansions in Floquet modes. The drawback is that the method can only handle cells with a single aperture. In this appendix it is shown how the method can be generalized to handle supercells.

Consider a frequency selective structure where the unit cell contains M apertures $\Omega_1, \Omega_2, \ldots, \Omega_M$. An example of such a cell with two different apertures; Ω_1 as an annular aperture, and Ω_2 as a a crossed dipole aperture, is given in Figure 5. The structure may contain dielectric layers on both sides of the metallic plate. In the regions outside the structure and in the dielectric layers, the fields are expanded in Floquet modes, whereas in the apertures the fields are expanded in waveguide modes. For general structures these modes are determined numerically by FEM. The waveguide mode amplitudes and the amplitudes for the Floquet modes are related to each other by scattering matrices. In this appendix it is shown how the

scattering matrix between the waveguide mode amplitudes and the Floquet mode amplitudes in an adjacent dielectric layer can be obtained.

The fields inside the dielectric layer are expanded in Floquet modes

$$
\begin{cases}
\boldsymbol{E}_{\mathrm{T}}^{\mathrm{a}}(\boldsymbol{r}) = \sum_{lmn} (a_{lmn}^{+} \mathrm{e}^{\mathrm{i}\gamma_{mn}^{\mathrm{a}}z} + a_{lmn}^{-} \mathrm{e}^{-\mathrm{i}\gamma_{mn}^{\mathrm{a}}z}) \boldsymbol{R}_{\mathrm{T}lmn}^{\mathrm{a}}(\boldsymbol{\rho}), \\
\boldsymbol{H}_{\mathrm{T}}^{\mathrm{a}}(\boldsymbol{r}) = \sum_{lmn} (a_{lmn}^{+} \mathrm{e}^{\mathrm{i}\gamma_{mn}^{\mathrm{a}}z} - a_{lmn}^{-} \mathrm{e}^{-\mathrm{i}\gamma_{mn}^{\mathrm{a}}z}) \boldsymbol{T}_{\mathrm{T}lmn}^{\mathrm{a}}(\boldsymbol{\rho}).
\end{cases}
\tag{B.1}
$$

The explicit expressions for the Floquet modes $\boldsymbol{R}_{\mathrm{T}lmn}^{\mathrm{a}}$ and $\boldsymbol{T}_{\mathrm{T}lmn}^{\mathrm{a}}$ are given in [7]. The fields inside the apertures are expanded in waveguide modes. In aperture Ω_i the expansion is

$$
\begin{cases}
\boldsymbol{E}_{\mathrm{T}}^{\mathrm{b}i}(\boldsymbol{r}) = \sum_{vn} (b_{vn}^{i+} \mathrm{e}^{\mathrm{i}k_{zn}^{\mathrm{b}i}z} + b_{vn}^{i-} \mathrm{e}^{-\mathrm{i}k_{zn}^{\mathrm{b}i}z}) \boldsymbol{E}_{\mathrm{T}vn}^{\mathrm{b}i}(\boldsymbol{\rho}), \\
\boldsymbol{H}_{\mathrm{T}}^{\mathrm{b}i}(\boldsymbol{r}) = \sum_{vn} (b_{vn}^{i+} \mathrm{e}^{\mathrm{i}k_{zn}^{\mathrm{b}i}z} - b_{vn}^{i-} \mathrm{e}^{-\mathrm{i}k_{zn}^{\mathrm{b}i}z}) \boldsymbol{H}_{\mathrm{T}vn}^{\mathrm{b}i}(\boldsymbol{\rho}),
\end{cases}
\tag{B.2}
$$

where the waveguide modes $\boldsymbol{E}_{\mathrm{T}vn}^{\mathrm{b}i}(\boldsymbol{\rho})$ are an orthonormal set of vector waves, *cf.* [7].

At the interface $z = z_0$ the tangential electric field is continuous over the entire interface D, while the magnetic field is continuous over the apertures, *i.e.*, the boundary conditions read

$$
\boldsymbol{E}_{\mathrm{T}}^{\mathrm{a}}(\boldsymbol{\rho}, z_0) = \begin{cases}
\boldsymbol{E}_{\mathrm{T}}^{\mathrm{b}i}(\boldsymbol{\rho}, z_0), & \boldsymbol{\rho} \in \Omega_i, i = 1, 2, \ldots, N, \\
\mathbf{0}, & \boldsymbol{\rho} \in D \setminus (\Omega_1 \cup \Omega_2 \cup \ldots \cup \Omega_N),
\end{cases}
\tag{B.3}
$$

$$
\boldsymbol{H}_{\mathrm{T}}^{\mathrm{a}}(\boldsymbol{\rho}, z_0) = \boldsymbol{H}_{\mathrm{T}}^{\mathrm{b}i}(\boldsymbol{\rho}, z_0), \quad \boldsymbol{\rho} \in \Omega_i, i = 1, 2, \ldots, N.
$$

Introducing

$$
\begin{aligned}
A_{lmn}^{\pm}(z) &= a_{lmn}^{\pm} \mathrm{e}^{\pm\mathrm{i}\gamma_{mn}^{\mathrm{a}}z}, \\
B_{vn}^{i\pm}(z) &= b_{vn}^{i\pm} \mathrm{e}^{\pm\mathrm{i}k_{zn}^{\mathrm{b}i}z},
\end{aligned}
\tag{B.4}
$$

and enforcing the continuity condition of the fields at the interface $z = z_0$ yield

$$
\begin{aligned}
\sum_{lmn} (A_{lmn}^{+}(z_0) + A_{lmn}^{-}(z_0)) \boldsymbol{R}_{\mathrm{T}lmn}^{\mathrm{a}}(\boldsymbol{\rho}) &= \begin{cases}
\sum_{vn} (B_{vn}^{i+}(z_0) + B_{vn}^{i-}(z_0)) \boldsymbol{E}_{\mathrm{T}vn}^{\mathrm{b}i}(\boldsymbol{\rho}), & \boldsymbol{\rho} \in \Omega_i, \\
\mathbf{0}, & \boldsymbol{\rho} \in D \setminus (\Omega_1 \cup \Omega_2 \cup \ldots \cup \Omega_N),
\end{cases} \\
\sum_{lmn} (A_{lmn}^{+}(z_0) - A_{lmn}^{-}(z_0)) \boldsymbol{T}_{\mathrm{T}lmn}^{\mathrm{a}}(\boldsymbol{\rho}) &= \sum_{vn} (B_{vn}^{i+}(z_0) - B_{vn}^{i-}(z_0)) \boldsymbol{H}_{\mathrm{T}vn}^{\mathrm{b}i}(\boldsymbol{\rho}), \quad \boldsymbol{\rho} \in \Omega_i.
\end{aligned}
\tag{B.5}
$$

To obtain a linear system of equations for the coefficients, the inner product is taken between Eq. (B.5a) and $\boldsymbol{T}_{\mathrm{T}l'm'n'}^{\mathrm{a}*}$, and between Eq. (B.5b) and $\boldsymbol{E}_{\mathrm{T}v'n'}^{\mathrm{b}i*}$, $i = 1, 2, \ldots, N$. The inner product integrals are

$$
\begin{aligned}
\mathbf{R}_{lmn,l'm'n'} &= \int_D \hat{z} \cdot (\boldsymbol{R}_{\mathrm{T}lmn}^{\mathrm{a}} \times \boldsymbol{T}_{\mathrm{T}l'm'n'}^{\mathrm{a}*}) \,\mathrm{d}S \\
&= \int_D \boldsymbol{R}_{\mathrm{T}lmn}^{\mathrm{a}} \cdot (\boldsymbol{T}_{\mathrm{T}l'm'n'}^{\mathrm{a}*} \times \hat{z}) \,\mathrm{d}S \\
&= \frac{Y_{l'm'n'}^{\mathrm{a}*}}{\eta_0} \int_D (\boldsymbol{R}_{\mathrm{T}lmn}^{\mathrm{a}} \cdot \boldsymbol{R}_{\mathrm{T}l'm'n'}^{\mathrm{a}*}) \,\mathrm{d}S = \frac{Y_{lmn}^{\mathrm{a}*}}{\eta_0} \delta_{ll'} \delta_{mm'} \delta_{nn'},
\end{aligned}
\tag{B.6}
$$

$$\mathbf{Q}^i_{vn,v'n'} = \int_{\Omega_i} \hat{z} \cdot (\boldsymbol{E}^{\mathrm{bi}}_{\mathrm{T}vn} \times \boldsymbol{H}^{\mathrm{bi}*}_{\mathrm{T}v'n'}) \, \mathrm{d}S = \frac{Y^{\mathrm{bi}*}_{vn}}{\eta_0} \delta_{vv'} \delta_{nn'}, \tag{B.7}$$

and

$$\begin{aligned}
\mathbf{C}^i_{vn,l'm'n'} &= \int_{\Omega_i} \hat{z} \cdot (\boldsymbol{E}^{\mathrm{bi}}_{\mathrm{T}vn} \times \boldsymbol{T}^{\mathrm{a}*}_{\mathrm{T}l'm'n'}) \, dS \\
&= \int_{\Omega_i} \boldsymbol{E}^{\mathrm{bi}}_{\mathrm{T}vn} \cdot (\boldsymbol{T}^{\mathrm{a}*}_{\mathrm{T}l'm'n'} \times \hat{z}) \, \mathrm{d}S = \frac{Y^{\mathrm{a}*}_{l'm'n'}}{\eta_0} \int_{\Omega_i} (\boldsymbol{E}^{\mathrm{bi}}_{\mathrm{T}vn} \cdot \boldsymbol{R}^{\mathrm{a}*}_{\mathrm{T}l'm'n'}) \, \mathrm{d}S,
\end{aligned} \tag{B.8}$$

where D is the entire surface of the cell. With these definitions, the linear system for the coefficients is

$$\begin{cases}
\mathbf{R}(\boldsymbol{A}^+ + \boldsymbol{A}^-) = \sum_i \mathbf{C}^t_i(\boldsymbol{B}^+_i + \boldsymbol{B}^-_i), \\
\mathbf{C}^*_i(\boldsymbol{A}^+ - \boldsymbol{A}^-) = \mathbf{Q}^*_i(\boldsymbol{B}^+_i - \boldsymbol{B}^-_i), \quad i = 1, 2, \ldots, N,
\end{cases} \tag{B.9}$$

The matrices $\mathbf{R}$ and $\mathbf{Q}_i$ are quadratic, but the matrix $\mathbf{C}_i$ is not necessarily quadratic. The linear system is rewritten as

$$\begin{cases}
\boldsymbol{A}^- = \sum_i \mathbf{R}^{-1}\mathbf{C}^t_i(\boldsymbol{B}^+_i + \boldsymbol{B}^-_i) - \boldsymbol{A}^+, \\
\boldsymbol{B}^+_i = \mathbf{Q}^{*-1}_i\mathbf{C}^*_i(\boldsymbol{A}^+ - \boldsymbol{A}^-) + \boldsymbol{B}^-_i \quad i = 1, 2, \ldots, N.
\end{cases} \tag{B.10}$$

The lower expression is inserted in the upper expression in (B.9). This gives

$$\mathbf{R}(\boldsymbol{A}^+ + \boldsymbol{A}^-) = \sum_i [\mathbf{C}^t_i \mathbf{Q}^{*-1}_i \mathbf{C}^*_i(\boldsymbol{A}^+ - \boldsymbol{A}^-) + 2\mathbf{C}^t_i \boldsymbol{B}^-_i]$$

$$\Leftrightarrow \quad (\mathbf{R} + \sum_i \mathbf{C}^t_i \mathbf{Q}^{*-1}_i \mathbf{C}^*_i)\boldsymbol{A}^- = -(\mathbf{R} - \sum_i \mathbf{C}^t_i \mathbf{Q}^{*-1}_i \mathbf{C}^*_i)\boldsymbol{A}^+ + 2\sum_i \mathbf{C}^t_i \boldsymbol{B}^-_i$$

$$\Leftrightarrow \quad \boldsymbol{A}^- = -(\mathbf{R} + \sum_j \mathbf{C}^t_j \mathbf{Q}^{*-1}_j \mathbf{C}^*_j)^{-1}(\mathbf{R} - \sum_j \mathbf{C}^t_j \mathbf{Q}^{*-1}_j \mathbf{C}^*_j)\boldsymbol{A}^+$$

$$+ 2(\mathbf{R} + \sum_j \mathbf{C}^t_j \mathbf{Q}^{*-1}_j \mathbf{C}^*_j)^{-1} \sum_i \mathbf{C}^t_i \boldsymbol{B}^-_i. \tag{B.11}$$

When this expression is inserted in the lower expression in (B.10) the following relation is obtained

$$\boldsymbol{B}^+_i = \mathbf{Q}^{*-1}_i \mathbf{C}^*_i [\mathbf{I} + (\mathbf{R} + \sum_j \mathbf{C}^t_j \mathbf{Q}^{*-1}_j \mathbf{C}^*_j)^{-1}(\mathbf{R} - \sum_j \mathbf{C}^t_j \mathbf{Q}^{*-1}_j \mathbf{C}^*_j)]\boldsymbol{A}^+$$

$$+ 2\mathbf{Q}^{*-1}_i \mathbf{C}^*_i(\mathbf{R} + \sum_j \mathbf{C}^t_j \mathbf{Q}^{*-1}_j \mathbf{C}^*_j)^{-1} \sum_k \mathbf{C}^t_k \boldsymbol{B}^-_k + \boldsymbol{B}^-_i. \tag{B.12}$$

By introducing a scattering matrix, the linear system can be written as

$$\begin{pmatrix} \boldsymbol{A}^- \\ \boldsymbol{B}^+_1 \\ \vdots \\ \boldsymbol{B}^+_N \end{pmatrix} = \begin{pmatrix} \mathbf{S}^{\mathrm{l}}_{1,1} & \mathbf{S}^{\mathrm{l}}_{1,2} & \cdots & \mathbf{S}^{\mathrm{l}}_{1,N+1} \\ \mathbf{S}^{\mathrm{l}}_{2,1} & \mathbf{S}^{\mathrm{l}}_{2,2} & \cdots & \mathbf{S}^{\mathrm{l}}_{2,N+1} \\ \vdots & \vdots & \ddots & \vdots \\ \mathbf{S}^{\mathrm{l}}_{N+1,1} & \mathbf{S}^{\mathrm{l}}_{N+1,2} & \cdots & \mathbf{S}^{\mathrm{l}}_{N+1,N+1} \end{pmatrix} \begin{pmatrix} \boldsymbol{A}^+ \\ \boldsymbol{B}^-_1 \\ \vdots \\ \boldsymbol{B}^-_N \end{pmatrix}, \tag{B.13}$$

where the elements of the scattering matrix are

$$
\begin{cases}
\mathbf{S}^{\mathrm{l}}_{1,1} = -(\mathbf{R} + \sum_j \mathbf{C}^t_j \mathbf{Q}^{*-1}_j \mathbf{C}^*_j)^{-1}(\mathbf{R} - \sum_j \mathbf{C}^t_j \mathbf{Q}^{*-1}_j \mathbf{C}^*_j), \\[2ex]
\mathbf{S}^{\mathrm{l}}_{1,i+1} = 2(\mathbf{R} + \sum_j \mathbf{C}^t_j \mathbf{Q}^{*-1}_j \mathbf{C}^*_j)^{-1}\mathbf{C}^t_i, \\[2ex]
\mathbf{S}^{\mathrm{l}}_{i+1,1} = \mathbf{Q}^{*-1}_i \mathbf{C}^*_i[\mathbf{I} + (\mathbf{R} + \sum_j \mathbf{C}^t_j \mathbf{Q}^{*-1}_j \mathbf{C}^*_j)^{-1}(\mathbf{R} - \sum_j \mathbf{C}^t_j \mathbf{Q}^{*-1}_j \mathbf{C}^*_j)], \\[2ex]
\mathbf{S}^{\mathrm{l}}_{i+1,i+1} = 2\mathbf{Q}^{*-1}_i \mathbf{C}^*_i(\mathbf{R} + \sum_j \mathbf{C}^t_j \mathbf{Q}^{*-1}_j \mathbf{C}^*_j)^{-1}\mathbf{C}^t_i + \mathbf{I}. \\[2ex]
\mathbf{S}^{\mathrm{l}}_{i+1,k+1} = 2\mathbf{Q}^{*-1}_i \mathbf{C}^*_i(\mathbf{R} + \sum_j \mathbf{C}^t_j \mathbf{Q}^{*-1}_j \mathbf{C}^*_j)^{-1}\mathbf{C}^t_k.
\end{cases}
\tag{B.14}
$$

This is the supercell correspondence of the single cell scattering matrix that is derived in [7]. The rest of the analysis used in [7] can now be applied.

References

[1] G. Arfken. *Mathematical Methods for Physicists*. Academic Press, Orlando, third edition, 1985.

[2] T. F. Eibert, J. L. Volakis, D. R. Wilton, and D. R. Jackson. Hybrid FE/BI modeling of 3-D doubly periodic structures utilizing triangular prismatic elements and an MPIE formulation accelerated by the Ewald transformation. *IEEE Trans. Antennas Propagat.*, **47**(5), 843–850, May 1999.

[3] H. Holter. *Analysis and Design of Broadband Phased Array Antennas*. PhD thesis, Royal Institute of Technology, Division of Electromagnetic Theory, S-100 44 Stockholm, Sweden, 2000.

[4] D. Sjöberg. Coherent effects in single scattering and random errors in antenna technology. Technical Report LUTEDX/(TEAT-7109)/1–21/(2002), Lund Institute of Technology, Department of Electroscience, P.O. Box 118, S-221 00 Lund, Sweden, 2002. `http://www.es.lth.se`.

[5] C.-H. Tsao and R. Mittra. Spectral-domain analysis of frequency selective surfaces comprised of periodic arrays of cross dipoles and Jerusalem crosses. *IEEE Trans. Antennas Propagat.*, **32**(5), 478–486, 1984.

[6] J. C. Vardaxoglou. *Frequency Selective Surfaces (Analysis and Design)*. Research Studies Press, 1997.

[7] B. Widenberg, S. Poulsen, and A. Karlsson. Scattering from thick frequency selective screens. *J. Electro. Waves Applic.*, **14**(9), 1303–1328, 2000.